Chapter 1
Self-action of Femtosecond Optical Vortex in a Medium with Kerr Nonlinearity

S. A. Shlenov, E. V. Vasilyev, V. P. Kandidov, A. A. Dergachev, and F. I. Soyfer

Abstract We numerically study the dynamics of the formation of optical vortex from collimated Gaussian beam behind a spiral phase plate, and assess the characteristic scale of azimuthal instability developing in a Kerr medium. The near zero values of intensity on axes arise shortly after the plate but the ring profile is formed at the distance of approximately half of the diffraction length. The break-up of the vortex into several hot spots in the Kerr medium is more rapid for the large-scale noise. The transformation of the vortex spatial spectrum is analyzed along with changes in its phase profile. The interference of the self-focusing mode and the radiation extending to the periphery leads to the formation of rings in the beam spectrum.

1.1 Introduction

The interest in the propagation of laser radiation in media with Kerr nonlinearity is largely due to the actual problems of femtosecond filamentation, during which extended high-intensity light filaments are formed [1]. The basis for the nucleation of filaments is the self-focusing of radiation in a medium with cubic nonlinearity [2, 3], which, together with other competing mechanisms, in particular, aberrational defocusing in self-induced plasma, ensures the maintenance of a high fluence in a bulk transparent medium at distances substantially longer than the diffraction (Rayleigh) length. Spatial effects are accompanied by a strong broadening of the frequency spectrum of the pulse. In media with anomalous group velocity dispersion due to

S. A. Shlenov · E. V. Vasilyev (✉) · V. P. Kandidov · A. A. Dergachev · F. I. Soyfer
Faculty of Physics and International Laser Center, M.V. Lomonosov Moscow State University, Leninskie Gori 1, Moscow 119991, Russia
e-mail: vasilev.evgeniy@physics.msu.ru

S. A. Shlenov
e-mail: shlenov@physics.msu.ru

V. P. Kandidov
e-mail: kandidov@physics.msu.ru

A. A. Dergachev
e-mail: aa.dergachev@physics.msu.ru

K. Yamanouchi et al. (eds.), *Progress in Photon Science*, Springer Series in Chemical Physics 125, https://doi.org/10.1007/978-3-030-77646-6_1

simultaneous spatial self-focusing and temporary self-compression of the pulse, the formation of wave packets with a high localization of the light field, the so-called "light bullets", is possible [4]. The phenomenon of filamentation can be considered as the basis of new laser technologies and applications related to the transmission of light energy with high fluence over long distances, the creation of remote white light sources, and the use of induced plasma channels of filaments [5].

The physical picture of femtosecond filamentation and the accompanying supercontinuum generation are well studied for the Gaussian and Bessel-Gaussian beams. However, more and more studies have recently appeared on the filamentation of beams of a more complex profile [6], including ring beams with a spiral phase dislocation on the axis—optical vortices [7], which can be described by the expression for the complex field amplitude using Lagger polynomials

$$E_{mn}(r, \varphi, z = 0) = E_0 \left(\frac{r}{r_0} \right)^m L_n^m \left(\frac{4r^2}{r_0^2} \right) \exp\left\{ -\frac{r^2}{2r_0^2} + im\varphi \right\}, \qquad (1.1)$$

where m is the topological charge, φ is the azimuthal angle, L_n^m—generalized n-order Laguerre polynomial, r_0 is the characteristic spatial scale. In the simplest case $L_0^m = 1$ the beam at $m > 0$ has the form of a ring, the inner and outer diameters of which depend on r_0 and m. Note that the absence of a topological charge ($m = 0$) transforms the formula (1.1) into an expression for a Gaussian beam of radius r_0. Vortex beams (1.1) have an orbital angular momentum and a helical phase front [7, 8], which prevents the "penetration" of the light field on the optical axis, where the zero-intensity point is located.

Optical vortex generation can be performed in various ways. It can be formed as a result of the interference of laser beams with an initially regular wavefront as they pass through randomly inhomogeneous media, optic fibers or specially made holograms [9]. In addition, the generation of vortex fields is possible directly in laser resonators [10]. It is relevant to obtain femtosecond vortices as ring beams with a phase dislocation in a wide frequency range typical for ultrashort pulses. In particular, dispersion-free schemes using uniaxial crystals and polarizing filters are proposed [11]. In principle, it is possible to use relatively simple spiral phase plates, passing through which collimated Gaussian beam acquires an annular intensity distribution with a phase dislocation on the axis [12].

The propagation of optical vortices in a linear medium has much in common with the diffraction of Gaussian beams. In [13], the behavior of the outer and inner radii of an optical vortex's ring-like profile as it propagated was analyzed, and a comparison was made with an experiment using a He-Ne laser. It was shown that the maximum intensity value at the diffraction length $z_d = kr_0^2$ both in the Gaussian and in vortex beams decreases by 2 times, and the width of the spatial profile increases by $\sqrt{2}$ times.

The study of self-focusing of optical vortices in a medium with cubic nonlinearity in the quasi-optical approximation was first performed in [14]. The critical power at which the self-similar solution corresponds to the collapse of the beam into an infinitely narrow ring was found. It was shown numerically and analytically that the critical power of an optical vortex increases with increasing topological charge m. The dependence of the critical power for self-focusing of the vortex beam $P_V^{(m)}$ on the topological charge m in units of the critical power of the Gaussian beam P_G is presented in [15]. For example, for $m = 1$ the critical power of optical vortex is $P_V^{(1)} = 4P_G$. Experimental confirmation of the increase in critical power with increasing m was obtained in [16] on the example of the optical vortices propagation in air.

It was shown in [17] that the collapse of a self-similar ring intensity distribution during self-focusing of an optical vortex can stop without additional competing mechanisms—only due to diffraction, which occurs during self-focusing of slit beams, corresponding to radial sections of vortex. One of the scenarios for further self-focusing of optical vortices is the formation of a thin high-intensity ring, which decreases in radius as it propagates.

In an experiment, the modulation instability in a cubic medium breaks the azimuthal symmetry of the beam, and it breaks up into individual hot spots—regions of filament formation. It was experimentally and numerically demonstrated that the presence of 10% amplitude-phase noise leads to the decay of a femtosecond vortex into several hot spots located along a circle, and the number of spots increases with increasing topological charge and pulse power [18]. In [19] it is shown that in a medium with the cubic-quintic nonlinearity optical vortices with a small topological charge are linearly stable, provided that they are very broad. In other words, we can get stable spinning spatio-temporal solitons as a result of the competition between focusing and defocusing nonlinearities [20]. Another opportunity to observe a stable propagation of the spatially localized single- and double-charge optical vortices in a self-focusing nonlinear medium is to use partially incoherent light [21].

It is significant for pulsed radiation that the azimuthal instability does not occur at the pulse front, where the instantaneous power is relatively small, and the optical vortex retains its axisymmetric shape in the intensity distribution [22]. Nevertheless, even when the intensity is high enough, so that the peak power exceeds the critical power of self-focusing, the breakup into hot spots occurs after the nonlinear focus [23] if the noise in the femtosecond vortex beam is small enough. This feature allows us to use the axisymmetric approximation for modeling the propagation of optical vortices at the initial stages of self-action. In [24], the decay of vortices with various topological charges under conditions of instantaneous and inertial plasma nonlinearity was studied. It is found that vortices with a topological charge $m = 1$ are more stable while propagating than vortices with a large topological charge. It was also found that the frequency of pulse refocusing increases with a topological charge of the beam.

Along with the spatiotemporal characteristics, the generation of the supercontinuum due to the self-action of optical vortices, particularly in calcium fluoride, has been studied. The vortex nature of the beam in the near and far zones are shown, and

the distribution of the spectral components of the radiation is obtained depending on the position of the beam waist relative to the input face of the crystal [25]. It was shown in [23] that, due to the high gradient of the intensity near the axis, the angular spectrum of the vortex beam is wider than that of the Gaussian beam with the same excess of the peak power over the critical value.

The propagation of femtosecond optical vortices under filamentation in a medium with anomalous group velocity dispersion was studied in the axisymmetric approximation in [26, 27]. It is shown that in the case of self-action of ring beams with a phase dislocation with a topological charge $m = 1$ in fused silica at a central wavelength $\lambda_0 = 1800$ nm, a sequence of annular light bullets with a duration of about 10 fs and a radius of at least 10 μm is formed. In this case, the radiation has a multifocus structure with the sharpest last focus, where global maxima of the intensity and plasma concentration on the propagation path are reached. Quantitative estimates of the transformation of the spectral energy of the pulse from the central region to the Stokes and anti-Stokes parts of the spectrum are obtained.

At the beginning of this paper, we numerically study the dynamics of the formation of optical vortices from Gaussian beam behind a spiral phase plate in order to evaluate the characteristic conversion distances and the possibility of using the same spiral phase plate to obtain optical vortices at adjacent wavelengths. Then we assess the characteristic scale of azimuthal instability development of the optical vortex in a medium with cubic nonlinearity, and, finally, analyze the features of transformation of its wave front and angular spectrum.

1.2 Vortex Formation from a Gaussian Beam in a Scheme with a Spiral Phase Plate

The most common laser beams used in experimental studies have Gaussian intensity profile (Fig. 1.1a) and plane or parabolic phase. To obtain an optical vortex we need to introduce the phase singularity into the phase profile (Fig. 1.1b), which can be done with the use of specific phase plates. Free propagation of the originally Gaussian beam with spiral phase, as we will show later, leads to a formation of an optical vortex having a ring-like intensity distribution (Fig. 1.1c).

To estimate lengths of propagation needed for the formation of the vortex, we used a 3D model of laser beam propagation:

$$2ik\frac{\partial A(x,y,z)}{\partial z} = \left[\frac{\partial^2}{\partial x^2} + \frac{\partial^2}{\partial y^2}\right]A(x,y,z) \tag{1.2}$$

The initial conditions for the slowly varying complex envelope $A(x, y, z = 0)$ were the following:

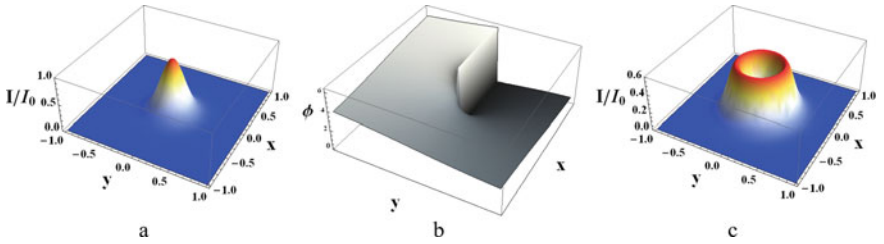

Fig. 1.1 Intensity distribution in the cross-section of the original Gaussian beam (**a**), the phase singularity in the beam after passing through the phase plate (**b**), intensity distribution in the cross-section of the optical vortex (**c**)

$$A(x, y, z = 0) = A_0 \exp\left\{-\frac{r^2}{2r_0^2}\right\} \exp\left\{im\varphi(x, y)\right\}, \tag{1.3}$$

where $r = \sqrt{x^2 + y^2}$, $\tan\varphi = y/x$. The topological charge of the vortex phase is $m = 1$ throughout the study. The beam radius is $r_0 = 1$ mm.

The simulation of the vortex propagation has several difficulties due to the phase singularity on the axis $x = y = 0$. In the formed vortex, the intensity of the laser field in the point of phase singularity is zero, but in our model, it is not zero right after the phase plate. The intensity near the axis rapidly declines and it reaches near zero values shortly after the plate. This is because of the destructive interference of the field at which the phase varies by 2π along the path enclosing the singularity. The ring-like intensity distribution is formed and is accompanied with the energy exchange between the central and peripheral parts of the beam which takes the form of ring-like waves from the central part to the peripheral, propagating at high angles to the optical axis. In numerical simulation, a finite computational grid is used so that these waves reaching the edges of the grid—reflect from them, return to the central part and interfere with the beam, producing numerical artifacts.

To overcome the problem of the indeterminate phase on the axis, phase jump is located between grid nodes (Fig. 1.2).

To overcome the interference with the reflected waves we extend the computational area in the cross-sectional dimensions so that there is some buffer areas around the beam for the ring waves to propagate farther from the beam. The typical grid has the size of 8192×8192 in the cross-section and the step along the propagation axis z is about 10^{-4} of the diffraction length $z_d = kr_0^2$, which allows us to correctly reproduce the initial stages of the beam evolution.

We compared the process of the vortex formation from the Gaussian beam after it passes through the phase plate and the propagation of the true vortex (see 1.1) with the same power. Their intensity profiles $I(r, \varphi = 0, z)$ are shown in Fig. 1.3. Shortly after the plate (Fig. 1.3a), the intensity profile of the beam is close to the original Gaussian form and far from the needed ring form of the vortex. At the distance $z = 0.01 z_d$ (Fig. 1.3b), the beam intensity in the area near the axis is close to zero and the peak intensity is higher than the original Gaussian beam due to the

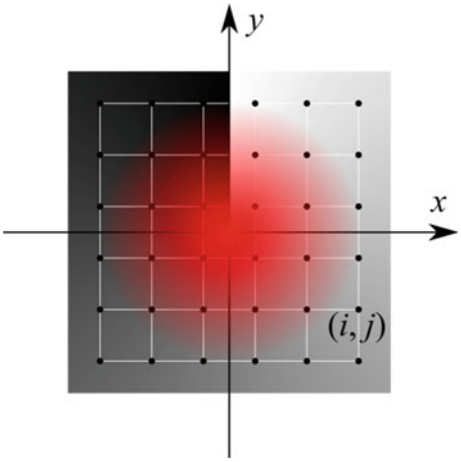

Fig. 1.2 The scheme of the Cartesian grid (black dots) used for numerical simulation of vortex formation behind the phase plate. The grayscale gradient represents the phase obtained after passing the plate. The initial Gaussian beam is shown in red. The picture does not show the scale of the used grid and beam size. The typical size of the grid was about several thousands of points along each cross-sectional coordinate

oscillations in the profile. The size of the low intensity area near the axis is also much smaller than for the vortex. At the distance $z = 0.5z_d$ (Fig. 1.3c), the beam in the simulation is very close to the vortex.

The radii of the optical vortex and the collimated Gaussian beam have the same dependence on the propagation distance in a linear medium:

$$r_v(z) = r_0\sqrt{1 + (z/z_d)^2}. \tag{1.4}$$

The radius of the beam in the simulation was defined as the distance from the beam axis and the position of the intensity global maximum. The obtained dependency of the beam radius on the propagation distance is shown in Fig. 1.4.

The analysis shows that the size of the ring and its profile reaches the expecting value at the distances of about $0.5z_d$. This value was taken as an estimate of the vortex formation distance.

We consider the use of spiral phase plate designed for the wavelength of 1800 nm to obtain an optical vortex in femtosecond pulses at this central wavelength. The wide spectrum of the femtosecond pulse means that the plate will be actually used for wavelengths different from those it was designed for. It leads to different phase shifts for different wavelengths in the spectrum. If the spectrum of the femtosecond pulse has a half-width of about 80 nm, a part of the femtosecond pulse whose wavelength is longer than the central wavelength by about 4.5% will also propagate through the same phase plate.

We conducted a series of numerical simulations using the phase plate designed for 1800 nm, producing a vortex with topological charge $m = 1$ at this wavelength. We used beams whose wavelengths are longer and shorter than 1800 nm. We found that there is up to 25% difference in the wavelength of the beam and of the plate when a clearly seen ring with a phase singularity is formed. Beams whose wavelengths are

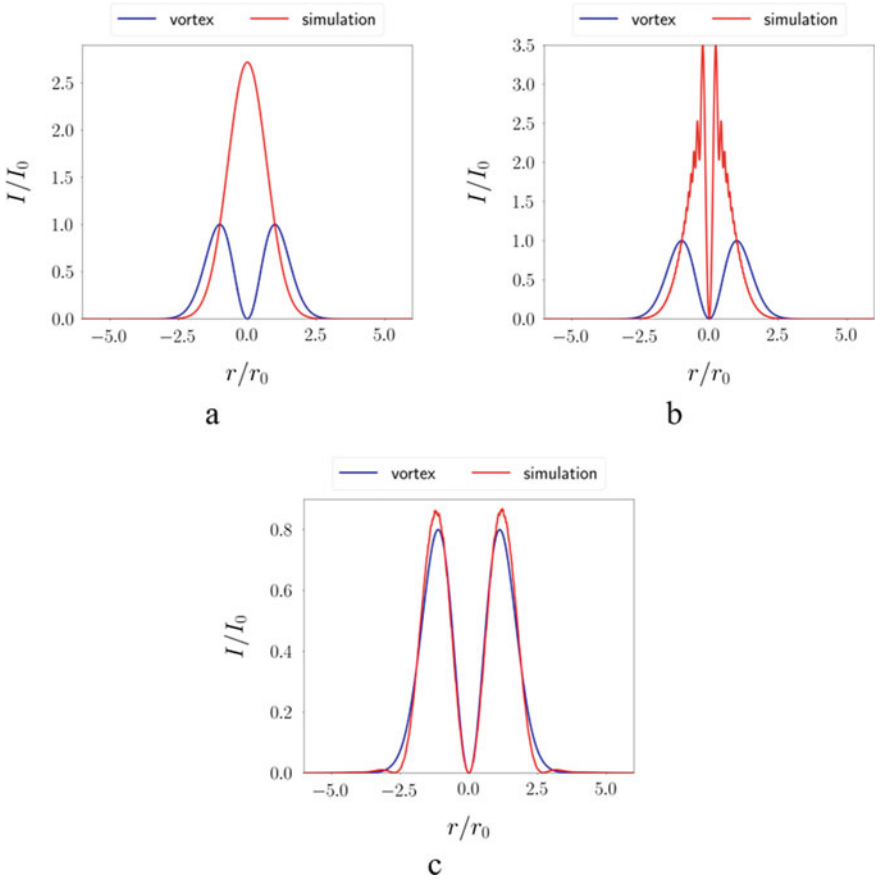

Fig. 1.3 Intensity profiles of the Gaussian beam after the spiral phase plate (red curves) and optical vortex (blue curves) at the distances $z/z_d = 0.00001$ (**a**), 0.01 (**b**), 0.5 (**c**); z_d is the diffraction length of the beam, I_0 is the vortex peak intensity at $z = 0$

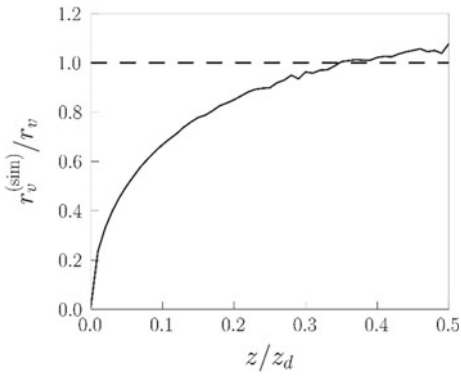

Fig. 1.4 The dependency of the beam radius obtained in simulation $r_v^{(sim)}$ and normalized by the radius of the vortex beam (1.5) $r_v(z)$ on the propagation distance z after the phase plate normalized by the diffraction length z_d. The dashed horizontal line stays for the radius of the optical vortex

longer than 2250 nm do not form a ring. Therefore, we hope that in the experiment the same spiral phase plate can be used to form a femtosecond optical vortex up to the central wavelength of 2100 nm.

1.3 Spatial Stability of the Optical Vortex in the Kerr Medium

The seed for the break-up of the vortex beam in Kerr medium is either a non-ideal beam profile or fluctuations of refractive index. We studied the process of the break-up for the laser beam of the form:

$$A^{(m)}(x, y, z = 0) = A_0 \left(\frac{r}{r_0}\right)^m \exp\left\{-\frac{r^2}{2r_0^2}\right\} \exp\left\{im\varphi(x, y)\right\}, \tag{1.5}$$

where $\tan\varphi = y/x$. The central wavelength was 1800 nm, the beam radius $r_0 = 92$ μm, topological charge $m = 1$. The peak intensity is $I_{max}(z = 0) = 1/e \times (cn_0A_0^2)/8\pi$, the beam power is $P = (cn_0A_0^2)/8\pi \times \pi r_0^2$, which is 5 times higher than the critical power of self-focusing for the vortex. In LiF crystal, for instance, the peak power would be 704 MW. For the 67 fs laser pulse, it corresponds to the total energy of 50 μJ.

The propagation equation for the complex envelope $A^{(m)}(x, y, z)$ (1.5) in the Kerr medium takes the form:

$$2ik\frac{\partial A(x, y, z)}{\partial z} = \left[\frac{\partial^2}{\partial x^2} + \frac{\partial^2}{\partial y^2} + \frac{2k^2}{n_0}n_2 I(x, y)\right] A(x, y, z) \tag{1.6}$$

This model is valid for the first stage of the pulse propagation, self-focusing, until the increasing intensity leads to the ionization of the medium. The intensity distributions in the cross-section of the beam at different propagation distances z obtained in the simulation illustrate the beam evolution in the nonlinear propagation process (Fig. 1.5). In the first stage the ring of the vortex exhibits self-contraction, i.e. its thickness decreases while the radius of the ring remains practically unchanged. The self-focusing in this stage does not lead to the beam collapse with the infinite increase in intensity even in the absence of defocusing factors like self-induced plasma or high-order nonlinearities. This is due to the fact that the energy concentrates only in one dimension (radial) so that it is similar to the self-focusing of the beam passed through a thin slit where the collapse is stopped by diffraction [17]. Therefore, the first nonlinear focus in the multi-focusing structure of the vortex filamentation can be achieved in the ionization-free regime [27].

At the distance $z = 0.8$ cm (Fig. 1.5c), a ring whose intensity is smaller than the main ring starts appearing in the peripheral part of the beam, being detached from the main ring, and the radius increases as the distance z increases.. After that, the radius of the main ring decreases and the new nonlinear focus is formed. The profile of the

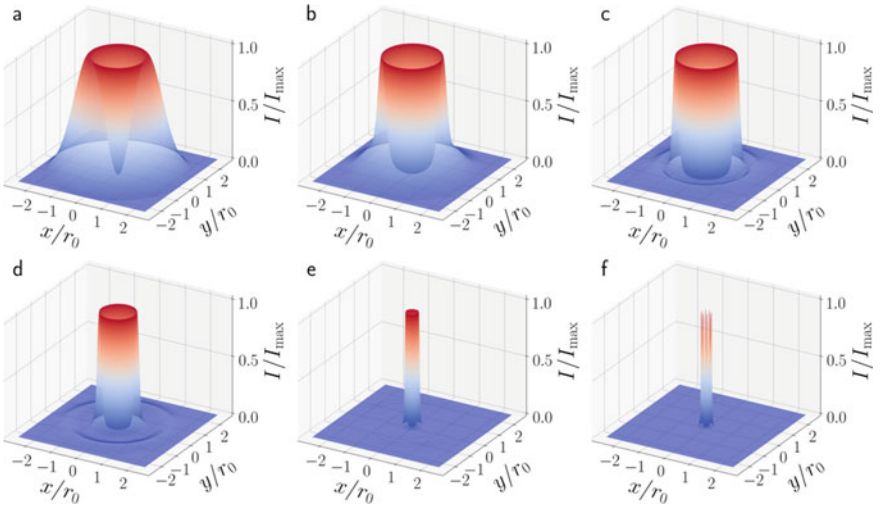

Fig. 1.5 Intensity distributions in the cross-section of the vortex at different distances z in the nonlinear medium: **a** 0 cm, **b** 0.6 cm, **c** 0.82 cm, **d** 1.36 cm, **e** 1.56 cm, **f** 1.58 cm. The intensity is normalized by its maximum at the given distance. The size of the shown region is 0.5 mm × 0.5 mm, total size of the grid is 1 mm × 1 mm

beam remains axially symmetric until $z = 1.58$ cm (Fig. 1.5f), where modulation instability leads to the break-up of the ring into several hot spots clearly separated in the azimuthal direction. Indeed, in the numerical simulation, the grid size is not fine enough even when we adopt ideal initial beam conditions with a uniform medium, that is, if the beam intensity becomes significantly large, a self-focusing proceeds, leading to a smaller cross-section of the beam than the grid size.

In the experimental conditions, the initial beam has spatial non-uniformities. Therefore the next series of calculations introduced some multiplicative noise $\xi(x, y)$ in the initial conditions. The noise was Gaussian. We used two values of its correlation radius r_c that differed by an order, which we hereafter call the large-scale ($r_c = 25$ μm) noise and the small-scale noise ($r_c = 2.5$ μm) (Fig. 1.6).

The total field amplitude had the form

$$A_{noise}(x, y, z = 0) = A^{(m)}(1 + \sigma\xi(x, y)), \tag{1.7}$$

where $A^{(m)}$ is defined by (1.5). The parameter σ was used to vary noise relative amplitude. Large-scale fluctuations near the intensity maximum in the ring contain the power of about $0.5P_{cr}$ for the Gaussian beam.

The discrepancy between maximum and minimum intensity at the same radius may be initially small but increases while propagating in nonlinear medium. To estimate the break-up quantitatively we introduced the decay coefficient $k_{decay}(z)$ as follows. We define the distance between the position of the intensity maximum and the beam axis as the ring radius $r_{ring}(z)$. We find the intensity minimum $I_{r,min}$ and

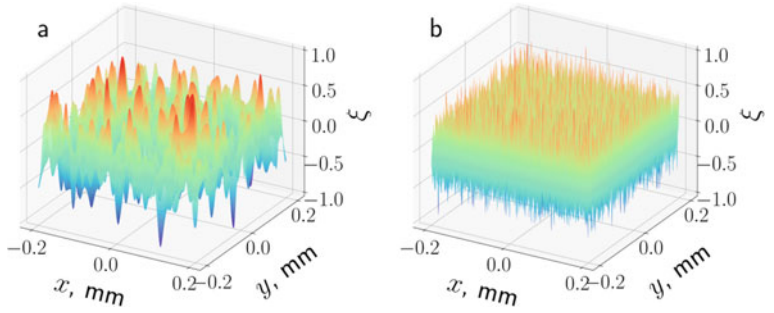

Fig. 1.6 The random noise distribution ξ in the initial conditions (1.7) with large-scale (**a**) and small-scale (**b**) noise

maximum $I_{r,max}$ over the circle centered on the beam axis with the radius $r_{ring}(z)$. The decay coefficient is defined as the relative difference between minimum and maximum intensity on the circle:

$$k_{decay}(z) = (I_{r,max} - I_{r,min})/I_{r,max} \tag{1.8}$$

For the ideal ring with constant intensity, the decay coefficient equals 0, for completely broken azimuthal symmetry it tends to be 1.

Figure 1.7 shows the dependence of the decay coefficient on the propagation distance. As it may be predicted, the increase in the noise ratio leads to the increase in modulation instability and earlier break-up, which holds both for the large- and small-scale noise. The value of the decay coefficient remains small until the propagation distance reaches about 0.1, beyond which it grows rapidly, leading to the abrupt break-up. The lesser the noise, the farther the beam propagates without break-up, and the more abrupt is the decay. In all the cases, the break-up occurred earlier than that in the noiseless beam. Therefore we proved that numerical instability and the grid noise in our simulations added little in comparison with the explicit noise in the initial conditions.

To estimate the distance to the visible break-up, we used the value z_{decay} at which $k_{decay} = 0.5$ (Fig. 1.8). The optical vortex brakes-up faster in the case of large-scale noise, because diffraction effectively smooths small-scale phase fluctuations.

1.4 Spatial Spectra of Annular Beams

We begin the analysis of angular spectra features of the optical vortices by considering the cross-section of the ring beam, which we set for simplicity as the sum of two Gaussian beams of width w located at distances ξ to the right and to the left of the point $x = 0$ (the axis of the ring beam):

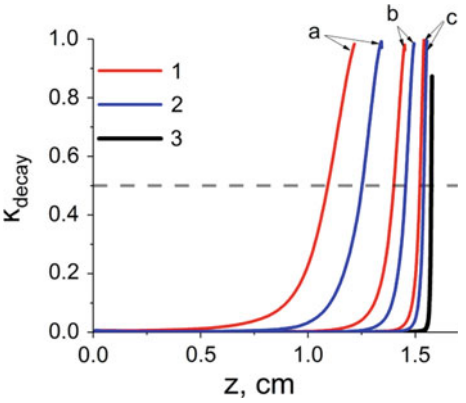

Fig. 1.7 The dependency of the decay coefficient k_{decay} from propagation distance z for large-scale noise (1), small-scale noise (2) and noiseless ($\sigma = 0$) vortex (3). Parameter $\sigma = 10^{-3}$ (**a**), 10^{-5} (**b**), 10^{-7} (**c**). The dashed line marks the threshold value which was used to determine the beam break-up distance

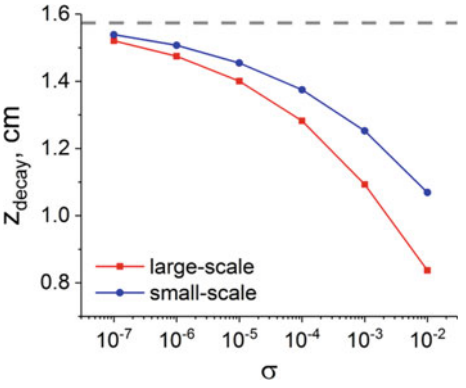

Fig. 1.8 The dependency of the break-up distance z_{decay} from the noise magnitude determined by σ for large-scale (red) and small-scaled (blue) noise. The dashed line marks the break-up distance for noiseless vortex (due to grid noise)

$$A(x) = A_0\left[\exp\left\{-\frac{(x-\xi)^2}{2w^2}\right\} + \exp\left\{-\frac{(x+\xi)^2}{2w^2}\right\}\right]. \tag{1.9}$$

We will assume that $\xi > w$. The spatial spectrum $S(k_x)$ of such a beam can be easily obtained analytically:

$$S(k_x) = 4w^2 \cos^2 k_x\xi \exp\left\{-(k_x w)^2\right\} \tag{1.10}$$

It has many local maxima ("spikes", in the two-dimensional case, rings) at spatial frequencies $k_x = n\pi/\xi, n = 0, \pm 1, \pm 2$. The distance between them is π/ξ, and their amplitude is modulated by a Gaussian envelope with characteristic width $1/w$. With an increase in the radius ξ, the width of each "spike" in the spectral space decreases, and their number within the envelope increases at a constant value of w. For clarity, Fig. 1.9 shows the beam profile and its spectrum for various values of ξ (a) and w (b).

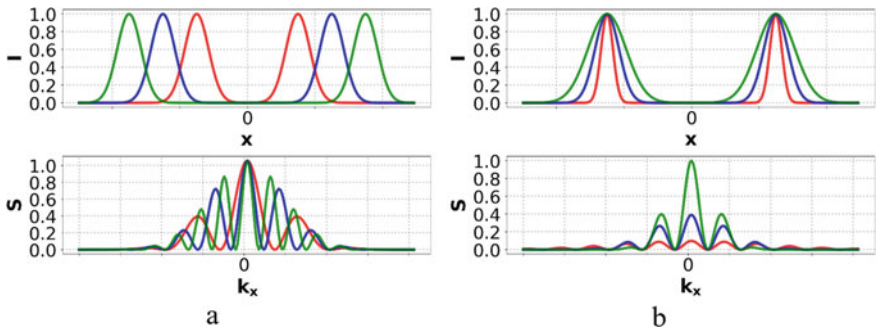

Fig. 1.9 The intensity distribution I of the diametrical cut of a three-dimensional ring beam (on the top) and the normalized spectral intensity S (at the bottom) for different beam radius ξ and ring width w

The behavior of the angular spectrum can be understood in terms of interference from two point sources, which are local maxima of the initial field distribution at distances ξ from the axis. The characteristic width of the interference fringes is inversely proportional to the distance between them. Therefore, the angular distance between the maxima decreases with increasing ξ.The smaller width w of the partial beams gives a wider spatial spectrum, that is the envelope width of local maxima in the spectrum grows and the spectral energy is redistributed to the region of high spatial frequencies. The relative magnitude of the central (global) maximum in the spectrum decreases.

In fact, the spatial distribution of intensity in the beam and its spectral components are visually similar to the radio pulse and its spectrum. Now the high-frequency packing and the envelope take place in the spectral space, and in ordinary coordinate space we have two maxima displaced with respect to zero, the width of which is determined by the width of envelope in the spectrum.

Similar conclusions are valid for a two-dimensional ring beam, but in this case one-dimensional local maxima will turn to rings. An important difference is that in the two-dimensional case one can also consider ring beams with a phase singularity on the axis, which leads to the disappearance of zero spatial harmonic in the spectrum. Instead, two maxima of smaller amplitude appear at spatial frequencies approximately corresponding to the first minimum in the spectrum for a beam without phase singularity. To illustrate the idea, consider a two-dimensional annular beam:

$$A_R(r) = A_0 \exp\left\{-\frac{(r-\xi)^2}{2w^2}\right\}, \tag{1.11}$$

where ξ is the radius of the ring, and w is its characteristic thickness. Adding a helical phase to (1.11) converts a collimated ring beam into an optical vortex, keeping the beam power unchanged:

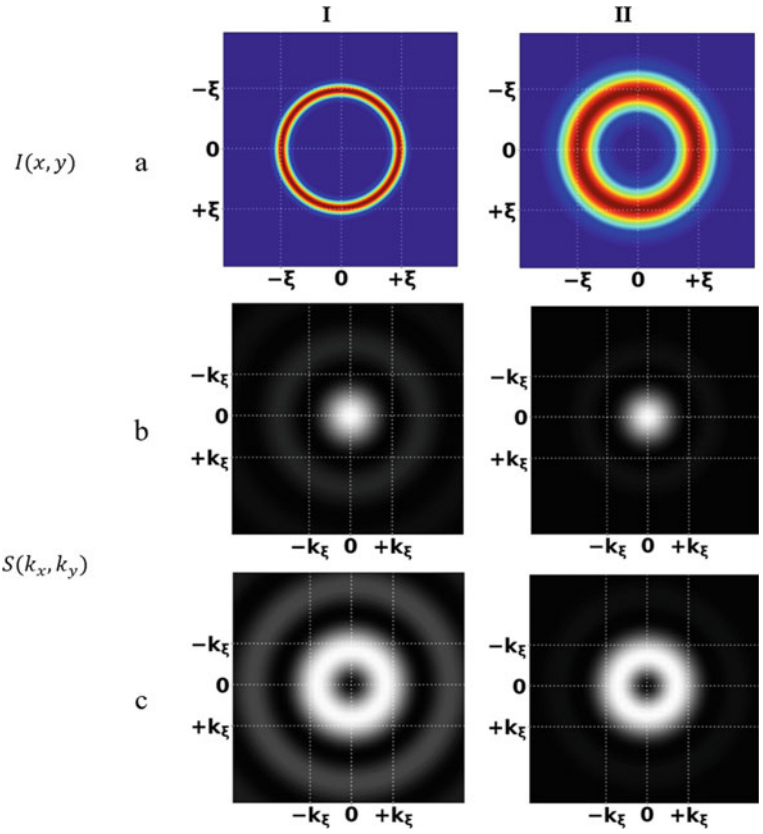

Fig. 1.10 Spatial distributions of the intensity $I(x, y)$ (**a**) and the spatial spectrum $S(k_x, k_y)$ for an annular beam without phase singularity (**b**) and for an optical vortex with a topological charge $m = 1$ (**c**) for a narrower ($w/\xi = 0.1$) (I) and wider ($w/\xi = 0.3$) (II) ring

$$A_V(r) = A_R \exp\left\{im\varphi(x, y)\right\}, \tag{1.12}$$

Figure 1.10 shows the intensity distributions $I(x, y)$ in the beam cross-section and its spatial spectra $S(k_x, k_y)$ for $w/\xi = 0.1$ (I) and 0.3 (II), where $\xi = 100$ μm. The spatial spectrum of the annular beam without phase singularity has a Bessel-like structure with a maximum at zero frequency and additional rings, the relative amplitude of which increases with decreasing width of the annular distribution of the beam intensity. At a relative ring width $w/\xi = 0.3$ (Fig. 1.10b, II), the spatial spectrum is almost unimodal—the second ring in it is very weak. In the case of a narrower ring with $w/\xi = 0.1$ μm, two additional rings with relatively low spectral intensity are clearly visible in the spectrum (Fig. 1.10b, I).

At the center of the spatial spectrum of the vortex there is always a minimum (Fig. 1.10c). It can be explained on the basis of the idea that at a distance ξ from

the optical axis there are many out-of-phase point sources of radiation. In particular, for an optical vortex with a topological charge $m = 1$, the out-of-phase sources are at the other end of the diameter. For a vortex beam with a relative ring thickness $w/\xi = 0.3\ \mu$m, the spatial spectrum has mainly one pronounced ring. As in the case of a ring beam without a phase singularity, a decrease in the parameter w leads to an increase in the relative spectral intensity in the secondary rings.

1.5 The Self-focusing Effect on the Wavefront and Spatial Spectrum of an Optical Vortex

The wavefront of the optical vortex (1.5) is a spiral isosurface $z = m/k\varphi(x, y)$, several steps of which are shown in Fig. 1.11a. Note that for $m = 0$, expression (1.5) describes a collimated Gaussian beam.

Intensity $I(x, y)$ and phase $\varphi(x, y)$ distributions in beam cross section of the optical vortex with $m = 1$ propagating in a linear medium are presented in Fig. 1.12 at various distances z. Hereinafter, the phase $\varphi(x, y)$ of the complex field $A = \Re[A] + i\Im[A]$ in the plane $z = const$ is calculated in the range of $-\pi$ to $+\pi$ as atan2($\Im[A], \Re[A]$). Because of the beam diffraction, boundary at which the phase jump occurs turns from a straight line into a curve spinning clockwise (Fig. 1.12b–d). A similar picture was observed the interferograms obtained after the diffraction of the Gaussian beam transmitted through a vortex plate [12].

Self-focusing of the optical vortex (1.5) can be described by a nonlinear wave equation (1.6). Consider an optical vortex with a topological charge $m = 1$ and a

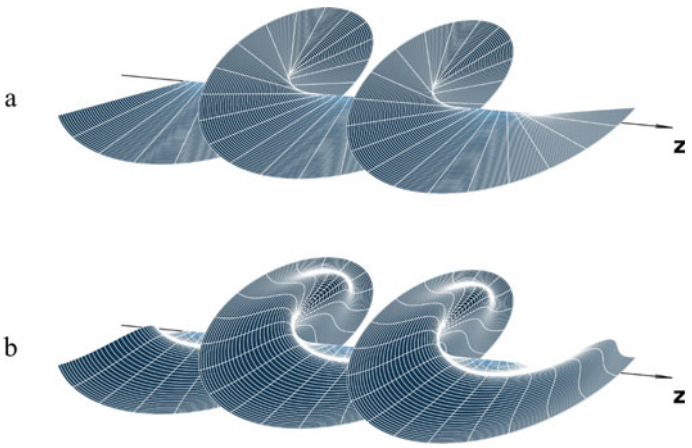

Fig. 1.11 The wavefront (phase isosurface) of the vortex beam at the beginning of the medium (**a**) and after self-focusing at a distance $z = 0.07z_d$ (qualitative picture, obtained in the approximation of a thin nonlinear lens) (**b**)

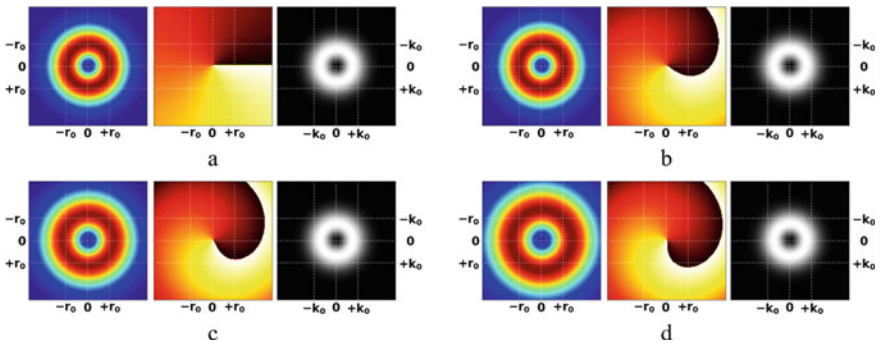

Fig. 1.12 Intensity (left), phase (center) and spectrum (right) distributions during optical vortex diffraction with a topological charge $m = 1$ at the beginning of the medium (**a**) and distances $z = 0.33$ (**b**), 0.66 (**c**) and 1.0 z_d (**d**) along the propagation direction $z_d = kr_0^2$

spatial parameter $r_0 = 100$ μm at a wavelength of $\lambda = 1800$ nm propagating in lithium fluoride. The excess of power over the critical value is chosen to be equal to $P/P_V^{(1)} = 5$, which corresponds to a nonlinear focus at a distance $z = 0.5z_d$ in the case of a Gaussian beam.

Figure 1.13 shows the intensity and phase spatial distribution of the beam, as well as its spatial spectra at different distances along the direction of the beam propagation. At the beginning of the medium (Fig. 1.13a), the intensity distribution has the form of a relatively wide ring with an e^{-2} width $w = 185$ μm, the phase across the beam has one jump by 2π, and one ring appears in the spatial (angular) spectrum. The self-action of an optical vortex begins with an increase in the peak intensity in the ring and a decrease in its width (Fig. 1.13b). Due to nonlinearity, the addition to the phase is larger in the high-intensity annular region; therefore, a phase jump of 2π does not occur along the radius across the beam. The boundary of the phase jump turns from a straight line into a curved one. The spiral surface of the wavefront in this case becomes convex (Fig. 1.11b), which corresponds to the stage of reducing the thickness of the ring intensity distribution. The twisting of the phase jump line at the periphery of the beam cross-section is associated with diffraction (Fig. 1.12).

Further propagation of the optical vortex twists counterclockwise the phase jump line in the beam cross section even more (Fig. 1.13c). Similar changes in the phase jump under self-focusing of the optical vortex were observed in [21]. Note that the direction of twisting is determined by the sign of the topological charge, i.e. in the case $m = -1$, the corresponding twist would be clockwise. In the spatial spectrum a small plateau forms on the outer side of the ring.

At a distance $z \sim 0.20z_d$ (Fig. 1.13d), the width of the ring in the intensity distribution achieves its minimum value, while the peak intensity reaches a local maximum (first nonlinear focus). At this distance, a decrease in the radius of the ring becomes noticeable, and the self-focusing mode of the optical vortex changes. A decrease in the width of the annular distribution while maintaining an almost constant average radius is replaced by a decrease in the radius when power is contracted to the axial

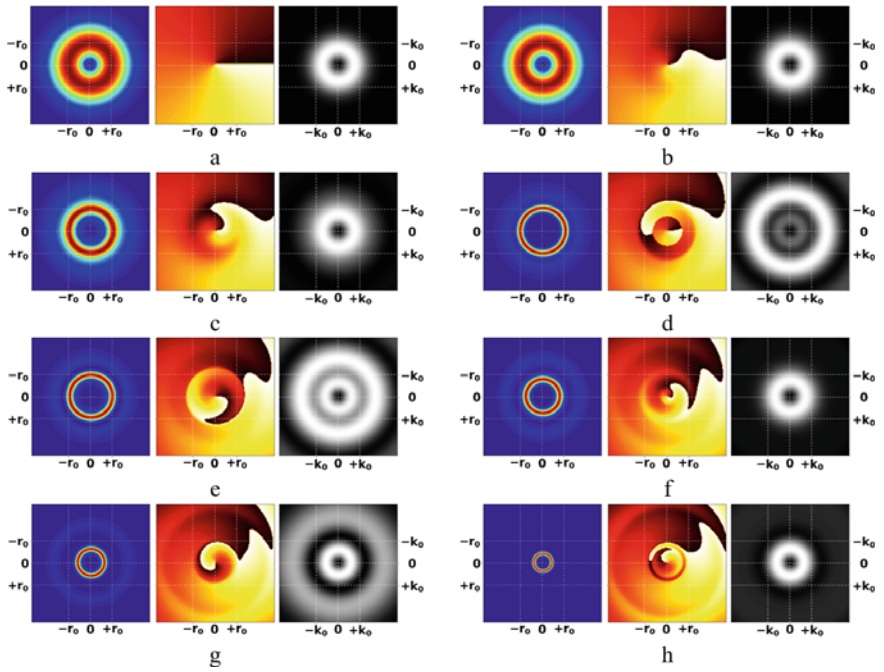

Fig. 1.13 The spatial distribution of the intensity $I(x, y)$ (left) and the phase $\theta(x, y)$ (center), and the spatial spectrum $S(k_x, k_y)$ (right) upon self-focusing of an optical vortex with a topological charge $m = 1$ at distances $z/z_d = 0.0$ (**a**), 0.07 (**b**), 0.14 (**c**), 0.20 (**d**), 0.25 (**e**), 0.31 (**f**), 0.36 (**g**), 0.43 (**h**) in nonlinear medium

region. In this case, aberrations appear on the beam profile—a new less intense ring appears, which, as the vortex propagates, shifts to the periphery of the beam, and the peak intensity of the main ring decreases.

Simultaneously, in the transverse distribution of the phase of the beam, three circular regions with distinct boundaries are formed, nested within each other along the aperture. In the inner circle, the phase behavior is similar to that of an optical vortex at the beginning of the medium (Fig. 1.13a). In the outer rings, the line of the phase jump is not straight but curved due to self-action, and resembles a spiral.

Hypothetically, these three regions can be related to the phase distributions of three different vortices of a limited aperture, nested in such a way that the vortex of a larger aperture is a continuation of the vortex of a smaller aperture. The phase of each of these spiral vortices is shifted by π relative to the closest vortex.

In the spatial spectrum of the optical vortex, the spectral intensity of the aberration rings increases. Moreover, the brightest ring with the highest spectral intensity is no longer the ring with the smallest radius. In the process of vortex propagation, the resulting spectrum is a superposition of partial spectra from each of the rings in the field distribution. An interference field from each of the rings is subject to a phase shift due to the formation of the embedded vortex structure in the phase. The vortex phase

leads to the absence of a central maximum in the spatial spectrum and the formation of a radiation cone around the optical axis. In Fig. 1.13d, the central low-intensity ring in the spectrum is generated by an external relatively wide, but low-intensity ring in the field distribution. The next high-intensity spectral ring is mainly the result of the high-intensity self-focusing mode formation, and the subsequent low-intensity rings in the spectrum are the result of the partial spectra addition from both rings in the field distribution.

We can explain the features of the formation of rings in the spectrum and their mutual intensity using a synthetic example. Let us consider a simple case of two out-of-phase embedded vortices with a topological charge $m = 1$ (Fig. 1.14). We set the field in the form of two ring beams of different radius ξ_{in} and ξ_{out} and a phase that experiences a jump at some distance from the axis of the beams:

$$A(r) = \begin{cases} A_{in} \exp\left\{-\frac{(r-\xi_{in})^2}{2w_{in}^2}\right\} \exp\left\{i \ \text{atan2}(x, y)\right\} & , \quad r \le \xi_{bound} \\ A_{out} \exp\left\{-\frac{(r-\xi_{out})^2}{2w_{out}^2}\right\} \exp\left\{i \ \text{atan2}(x, y) + \pi/m\right\} & , \quad r > \xi_{bound}, \end{cases} \tag{1.13}$$

where the values A_{in} (A_{out}), w_{in} (w_{out}) describe the amplitude and width of the inner and outer rings, respectively. This field distribution can be named as two nested vortices. Let the circle boundary of the phase shift be at a distance from the axis equal to $\xi_{bound} = 0.5(\xi_{in} + \xi_{out})$. The radii and widths of the rings are chosen so that they are far enough from each other and do not overlap: $\xi_{in} = 100$ μm, $w_{in} = 10$ μm, $\xi_{out} = 300$ μm, $w_{out} = 50$ μm. The initial field distribution (1.13) assumes that the radiation from the inner ring has one vortex phase, and the outer ring has the other, shifted by π.

The spatial spectrum of the field (1.13) also has two pronounced rings. The inner spectral ring corresponds to smaller angles of divergence of radiation, i.e. to the larger ring in the intensity distribution, and vice versa. The spectral intensity of the outer ring in the spectrum depends on the field amplitude in the inner ring. The ratio of amplitudes at fixed radii and widths of the rings determines their spectral intensities. With $A_{in} = 5A_{out}$, the intensity of the rings in the spectrum coincides (Fig. 1.14b). Deviation from the indicated ratio up (Fig. 1.14a) or down (Fig. 1.14c) results in the outer or inner ring having a higher spectral intensity. In Fig. 1.13d, the transverse field distribution formed during the self-focusing of the vortex is similar to distribution (1.13). However, in this phase there are three ring regions with clear boundaries. Each of these regions generates its spectral ring, the most intense of which corresponds to the middle spiral vortex, since the field with the largest amplitude is contained within its aperture.

It should be noted that the width of the central minimum in spatial spectrum increases with increasing topological charge. The nature of the pattern of maxima and minima depends on the parameters of the vortex. The angular distance between the maxima of the neighboring rings in the spectrum increases with the radius of the vortex ring. The wider the spectrum, the smaller the width of the ring in the beam. Since the optical vortex propagation is associated with the appearance of two modes:

one that is self-focusing and the other that spreads to the periphery, the resulting spectrum is the superposition of the ring systems that each mode generates.

Ongoing self-focusing of the optical vortex leads to a change in the twisting structure of the phase distribution. The internal and middle spiral vortices become in-phase and merge into one at a distance $z \sim 0.25 z_d$ (Fig. 1.13e). Moreover, the corresponding rings in the spatial spectrum become similar in amplitude and practically merge. The radius of the self-focusing mode continues to decrease, and the intensity becomes larger. The distance to the outer low-intensity ring increases. The internal spiral vortex becomes in phase with the external spectral vortex, i.e. the

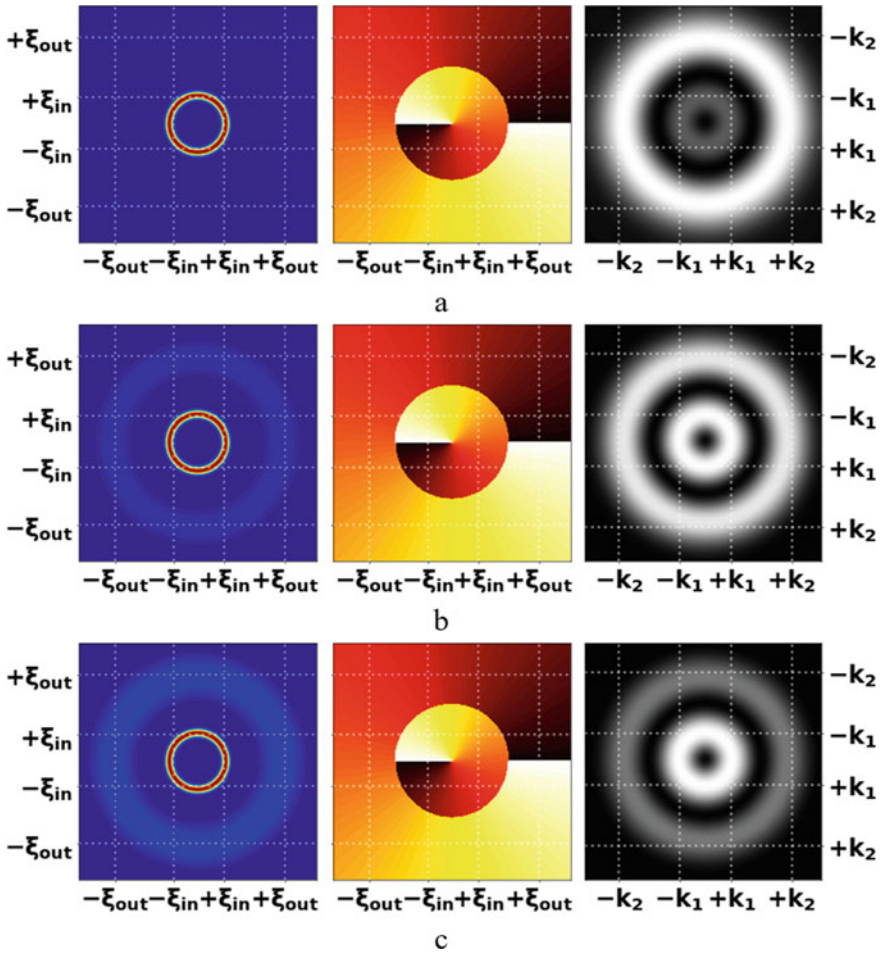

Fig. 1.14 The spatial distribution of the intensity $I(x, y)$ (left), phase $\varphi(x, y)$ (in the center) and the spectrum $S(k_x, k_y)$ (right) of the optical vortex defined by formula (1.13) with the ratio of the coefficients field amplitudes of the inner and outer rings $A_{in}/A_{out} = 10$ (**a**), 5 (**b**) and 2.5 (**c**)

spatial phase distribution becomes similar to the initial spectral vortex, only with a strongly curved line of the phase jump (Fig. 1.13f). The spatial spectrum of radiation is also similar to those of the initial vortex, i.e. it has a pronounced single ring. At a distance $z \sim 0.36 z_d$ (Fig. 1.13g), the distribution of the intensity and that of the phase become very similar to the synthetic example considered above (Fig. 1.14b), i.e. two distinctly spaced rings with different intensities and two embedded spiral vortices give rise to two spatial spectral rings with approximately the same brightness. Further propagation of the optical vortex (Fig. 1.13h) is accompanied by a decrease in the radius of the central ring and the periodic appearance of nested spiral vortices in the phase distribution.

1.6 Conclusion

We studied the process of the vortex formation after the spiral phase plate. We found that the near zero values of the intensity on the axes arise shortly after the plate but the ring profile is formed much further at the distance of approximately half of the diffraction length. A better idea would be to produce the vortex in the waist of the focused beam. The spectral width of the femtosecond pulse is not an obstacle for the vortex formation. We showed that we could separate the effects of noise in the initial conditions and the grid noise for typical sizes of the computational grid. The break-up of the vortex into several hot spots in the Kerr medium due to modulation instability is more rapid for the large-scale (in the conditions of the simulation) noise. The revealed features of transformation of the phase profile of the optical vortex and its spatial spectrum in a Kerr medium can be used in the analysis of spectral broadening in the filamentation mode.

Self-focusing of the optical vortex was analyzed in detail. It is shown that in the process of nonlinear propagation of a vortex beam, embedded spiral vortices appear in the phase distribution. The constructive interference of the self-focusing mode and the ring extending to the periphery leads to the formation of rings in the beam spatial spectrum.

Acknowledgements This research was supported by the Russian Foundation for Basic Research, grant 18-02-00624, and was carried out using the equipment of the shared research facilities of HPC computing resources at Lomonosov Moscow State University.

References

1. V.P. Kandidov, S.A. Shlenov, O.G. Kosareva, Filamentation of high-power femtosecond laser radiation. Quantum Electron. **39**(3), 205–228 (2009)
2. G.A. Askaryan, The effect of the field gradient of an intense electromagnetic beam on electrons and atoms. JETP **42**, 1567 (1962)

3. R.Y. Chiao, E. Garmire, C.H. Townes, Self-trapping of optical beams. Phys. Rev. Lett. **13**, 479 (1964)
4. L. Berge, S. Skupin, Few-cycle light bullets created by femtosecond filaments. Phys. Rev. Lett. **100** (2008)
5. J. Kasparian, J.-P. Wolf, Physics and applications of atmospheric nonlinear optics and filamentation. Opt. Express **16**(1), 466 (2008)
6. P. Polynkin, M. Kolesik, J. Moloney, Opt. Express **17**(2), 575–584 (2009)
7. V.V. Kotlyar, A.A. Kovalev, *Accelerated and Vortex Laser Beams* (FIZMATLIT, Moscow, 2018), p. 256
8. L. Allen et al., Orbital angular momentum of light and transformation of Laguerre Gaussian laser modes. Phys. Rev. A **45**(11), 8185–8189 (1992)
9. Z.S. Sacks, D. Rozas, G.A. Swartzlander, Holographic formation of optical-vortex filaments. J. Opt. Soc. Am. B **15**(8), 2226–2234 (1998)
10. L.E. Grin, P.V. Korolenko, N.N. Fedotov, On the generation of laser beams with a helical wavefront structure. Opt. Spectrosc. **73**(5), 1007–1010 (1992)
11. V.G. Shvedov, C. Hnatovsky, W. Krolikowski, A.V. Rode, Efficient beam converter for the generation of high-power femtosecond vortices. Opt. Lett. **35**(15), 2660–2662 (2010)
12. V.V. Kotlyar, A.A. Kovalev, R.V. Skidanov, S.N. Khonina, O.Yu. Moiseev, V.A. Soifer, Simple optical vortices formed by a spiral phase plate. J. Opt. Technol. **74**, 686–693 (2007)
13. S.G. Reddy, C. Permangatt, S. Prabhakar, A. Anwar, J. Banerji, R.P. Singh, Divergence of optical vortex beams. Appl. Opt. **54**, 6690–6693 (2015)
14. V.I. Kruglov, Yu.A. Logvin, V.M. Volkov, The theory of spiral laser beams in nonlinear media. J. Mod. Opt. 2277–2291 (1992)
15. L.T. Vuong, T.D. Grow, A. Ishaaya, A.L. Gaeta, G.W. Hooft, E.R. Eliel, G. Fibich, Phys. Rev. Lett. **96** (2006)
16. P. Polynkin, C. Ament, J.V. Moloney, Phys. Rev. Lett. **111** (2013)
17. E.V. Vasiliev, V.P. Kandidov, V.O. Kompanets, S.V. Chekalin, S.A. Shlenov, Formation of annular light bullets in a femtosecond vortex beam. Bull. Russ. Acad. Sci. Phys. **83**(12), 1443–1449 (2019)
18. A. Vincotte, L. Berge, Femtosecond optical vortices in air. Phys. Rev. Lett. **95** (2005)
19. I. Towersa, A.V. Buryaka, R.A. Sammuta, B.A. Malomedb, L.-C. Crasovanc, D. Mihalachec, Phys. Lett. A **288**, 292–298 (2001)
20. D. Mihalache, D. Mazilu, L.-C. Crasovan, I. Towers, A.V. Buryak, B.A. Malomed, L. Torner, J.P. Torres, F. Lederer, Stable spinning optical solitons in three dimensions. Phys. Rev. Lett. **88** (2002)
21. C.-C. Jeng, M.F. Shih, K. Motzek et al., Phys. Rev. Lett. (2004)
22. G. Maleshkov et al., Proc. SPIE (2009)
23. R.A. Vlasov, V.M. Volkov, D.Yu. Dedkov, Spectrum superbroadening in self-focusing of pulsed vortex beams in air. Quantum Electron. **43**(2), 157–161 (2013)
24. O. Khasanov, T. Smirnova, O. Fedotova, G. Rusetsky, O. Romanov, High-intensive femtosecond singular pulses in Kerr dielectrics. Appl. Opt. **51**, 198–207 (2012)
25. D.N. Neshev et al., Supercontinuum generation with optical vortices. Opt. Express **18**(17), 18368–18373 (2010)
26. E.V. Vasilyev, S.A. Shlenov, V.P. Kandidov, Annular light bullets of a femtosecond optical vortex in a medium with anomalous group velocity dispersion. Laser Phys. Lett. **15**, 115402–115407 (2018)
27. E.V. Vasilyev, S.A. Shlenov, V.P. Kandidov, The Multifocus structure of radiation upon femtosecond filamentation of an optical vortex in a medium with an anomalous group velocity dispersion. Opt. Spectrosc. **126**(1), 24–31 (2019)